J. Fluid Mech. (1992), *vol.* 240, *pp.* 601–625
Printed in Great Britain

Some aspects of mixing in a stratified turbulent patch

By I. P. D. DE SILVA AND H. J. S. FERNANDO
Department of Mechanical and Aerospace Engineering, Arizona State University, Tempe, AZ 85287-6106, USA

(Received 2 July 1991 and in revised form 3 January 1992)

Mixing in a turbulent patch, that was generated within a linearly stratified fluid of buoyancy frequency N_0, was studied experimentally. The turbulence within the patch was induced by sustained oscillations of a mono-planar grid. Grid oscillations produced a local turbulent region, which initially grows rapidly as in a non-stratified fluid and then assumes a quasi-stationary thickness $(L_p)_c$ when the stratification inhibits its vertical growth at a time $N_0 t \approx 4$. The growth beyond $(L_p)_c$ occurs slowly via breaking of interfacial waves at the entrainment interface. As mixing proceeds, the buoyancy frequency within the patch N decreases. The time evolution of N, the buoyancy lengthscale, the Thorpe lengthscale, the maximum Thorpe displacement, the overturning lengthscale and the available potential energy fluctuations were measured and their relationships were investigated. Various aspects of the wave radiation from the patch to the outer stratified layer, the trapping of interfacial waves at the entrainment interface, and the effects of grid parameters on the evolution of the patch were also studied.

1. Introduction

It is well known that stable stratification inhibits the vertical growth of turbulent regions. As a result, turbulence in stratified media is confined to patches whose horizontal scale is much larger than the vertical scale. Specific examples are demonstrated by the oceanic measurements of Nasmyth (1970, 1972) and Dugan (1984), which show mixed patches that have horizontal and vertical scales of several kilometres and several metres, respectively. Since mass and momentum transfers in stably stratified turbulence are largely determined by the characteristics of these patches (Barenblatt 1982), there is a considerable interest in studying their behaviour. The goal is to develop accurate parameterizations for the dynamical processes occurring within such regions.

Stratified turbulent patches are often characterized by the presence of small-scale density inversions (local regions with unstable density distributions), that are caused by overturning motions, in which heavy fluid particles are lifted (and light particles are lowered) by inertia forces associated with turbulent eddies. The extent of these vertical displacements depends on the relative strengths of the inertia and buoyancy forces. Hence, commonly used lengthscales for stratified turbulence are based on the r.m.s. fluctuations of buoyancy and velocity, and characteristics of the inversions measured at a given time.

The aim of the present study is to generate an isolated turbulent patch in a linearly-stratified fluid under controlled laboratory conditions and to study the relations between some generic parameters, especially those useful in characterizing

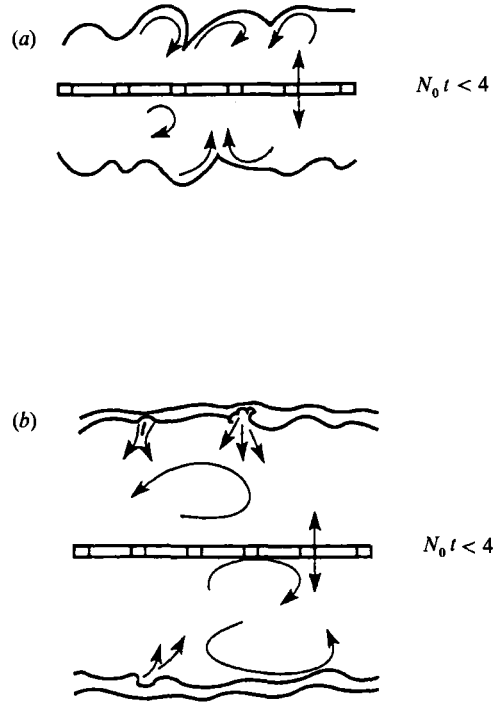

FIGURE 1. (*a*) A schematic diagram representing the initial growth mechanism. Here the turbulent eddies are sufficiently energetic to engulf the non-turbulent fluid. (*b*) The entrainment mechanism during the 'subsequent growth'. In this case the eddies cannot overturn and tend to flatten at the density interface. The growth occurs by the breaking of interfacial waves.

turbulent mixing. A horizontal confined mono-planar grid that performs sustained vertical oscillations in a salinity-stratified fluid was used as the experimental flow configuration. This enables us to obtain a well-defined patch whose evolutionary state is known. A similar experimental configuration was used by Fernando (1988) to study the growth rate of a stratified turbulent patch but, in that study, no measurements of turbulent parameters were made.

According to Fernando (1988), once the grid oscillations are started, two turbulent fronts propagate away from the grid thus forming a growing turbulent region. Initially, the growth of the patch follows the corresponding growth law for non-stratified fluids, and buoyancy effects play a negligible role. Entrainment occurs by the engulfment of non-turbulent fluid by the turbulent eddies and the turbulent/non-turbulent front (entrainment interface) is contorted. This rapid growth regime, which lasts for a non-dimensional time of $N_0 t \approx 4$, where N_0 is the background buoyancy frequency, is called the *initial growth* regime (see figure 1*a*). At $N_0 t \approx 4$, the buoyancy forces exert a retarding effect on the growth of the patch, and the patch growth is temporarily halted. The size of the patch at this stage is called the *critical size* of the patch. Thenceforward, the patch growth is very slow and takes place by breaking of interfacial waves that are generated at the interface (see figure 1*b*). The breaking events cause isolated (secondary) turbulent patches, which merge with the primary patch, thus increasing its size. Unlike in the initial growth regime, the eddies in the patch are now too feeble to engulf the ambient non-turbulent fluid.

The turbulent-front propagation for the present flow configuration has been analysed by Redondo (1990). It was shown that the turbulent fronts adjust so as to

propagate symmetrically with respect to the mid-plane of the grid. Hannoun, Fernando & List (1988) made detailed measurements near density interfaces and showed that the influence of the interface vanishes at distances greater than the integral lengthscale of turbulence. Since the turbulent fronts are separated by several integral scales (§3), it can be expected that they propagate quite independently of each other. The tendency for the fronts to propagate symmetrically with respect to the grid should not be construed as a consequence of a strong dynamical interdependence between the fronts: the nature of turbulent velocity and lengthscale distributions within the patch and the entrainment law are mainly responsible for the adjustment of the front to a common speed.

Section 2 of this paper is devoted to a description of the experimental procedure. Measurements of grid-generated turbulence in homogeneous fluids, which are used to calibrate the grid for its turbulence-generating properties, are given in §3. Qualitative observations and quantitative measurements pertinent to the stratified experiments are discussed in §4. The paper closes with a summary of results and a discussion of their possible application to geophysical situations.

2. Experiment

Schematic diagrams of the experimental apparatus are shown in figure 2. The experiments were conducted in a Plexiglas tank of square cross-section (26 cm × 26 cm) and a height of 60 cm. The cross-section of the tank is similar to that used by Thompson & Turner (1975), although the present tank is taller. The turbulence-producing grid was suspended inside the tank, using stainless-steel rods of 0.5 cm diameter, at a height of 25 cm from its bottom. The grids fit into the tank with 3 mm clearance with the sidewalls. The suspension rods were connected to a horizontal template which, in turn, was connected to a slider-crank mechanism driven by a variable speed, high-traction motor via an eccentric wheel. Three grids with different mesh sizes, made of square Plexiglas bars of cross-section ($d \times d$) 9 mm × 9 mm were used; the mesh sizes were $M = 6.20$ cm (solidity 27%), $M = 4.76$ cm (solidity 36%) and $M = 2.93$ cm (solidity 50%). Two strokes $S = 0.85$ cm and 2.1 cm, were used. The frequency of the grid oscillations f was varied over the range $1 < f < 5$ Hz.

The density measurements were made using a commercial microscale conductivity probe manufactured by Precision Measurement Engineering. The spatial resolution and the frequency-response cutoff of the probe were estimated to be 4 cycles cm^{-1} and 800 Hz, respectively (Head 1983). A similar probe has been used by Itsweire (1984) to obtain the instantaneous vertical structure of density in a stratified water channel. The probe was attached to a vertically traversing platform, and was capable of plunging into the fluid system with a preset speed of 50 cm s^{-1} and returning to its original setting at 0.5 cm s^{-1}. The platform travels on a precision translator between microswitch-controlled end limits and is powered by a stepping motor. The position of the probe was monitored by a precision potentiometer. A steel structure, independent of the deck that supports the oscillating mechanism, was used to position the traversing platform above the tank. An additional, stationary (manually adjustable) conductivity probe was also attached to the same steel structure to measure the density fluctuations within the patch. The density probes, oscillating mechanism and the experimental tank were mounted on separate platforms to isolate vibrations.

The horizontal and vertical turbulent velocities in homogeneous water were

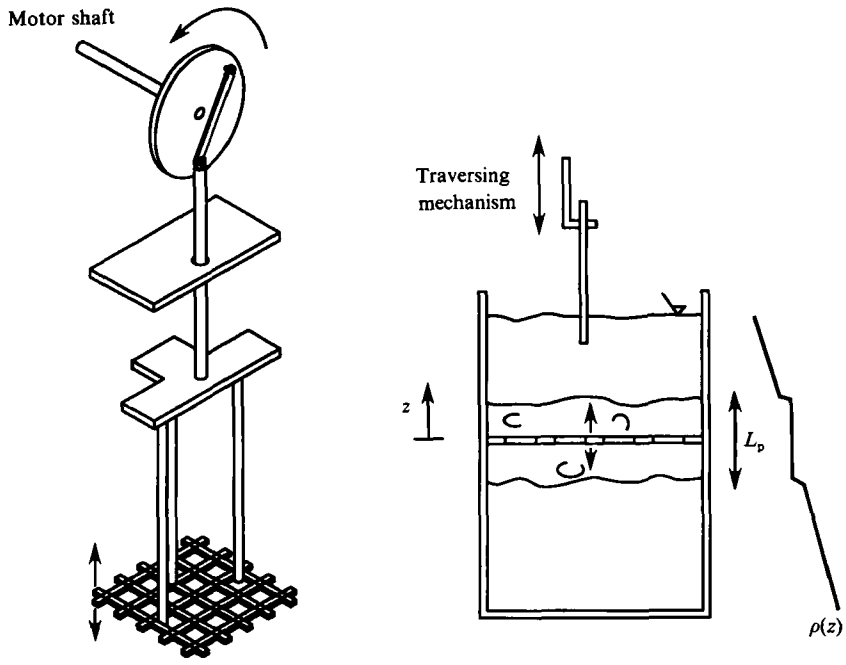

FIGURE 2. Schematic diagrams of the experimental apparatus. (*a*) Oscillating-grid mechanism; (*b*) experimental tank.

measured using a single-component laser-Doppler velocimeter (TSI model 9100-3), operating in the forward-scatter mode. To reduce the velocity bias (Durao, Laker & Whitelaw 1980) and to avoid corrections for the mean and fluctuating velocities (McLaughlin & Tielderman 1973), the data sampling frequency was kept at approximately 5–10 % of the data rate of the signal processor; sometimes to satisfy this criterion additional seeding was necessary. Time traces were typically 100 s long with a sampling frequency of 50 Hz. In calculating the r.m.s. velocity, the data were corrected for noise by assuming the velocity signal and the noise to be uncorrelated; a correction of the form $\overline{u}^2_{\text{turb}} = \overline{u}^2_{\text{meas}} - \overline{u}^2_{\text{noise}}$ was applied. The noise level was measured to be $\overline{u}^2_{\text{noise}} = 1.6 \times 10^{-3}$ cm^2 s^{-2}, and the minimum velocity measured was three times the noise level.

The data acquisition was performed using a Metrabyte Dash8 A/D board and the data were stored in a microcomputer for subsequent analysis. The flow visualization was performed by adding a small amount of fluorescein to the patch and illuminating it with an Argon-ion laser sheet. In some cases, a shadowgraph was also used for visualization purposes.

Two types of experiment were performed. One set was carried out in homogeneous distilled water to study grid-generated turbulence without stratification. This set of experiments could be considered as a calibration for the turbulence source (oscillating grid), which can be used to interpret the results of the second set of experiments carried out in salt-stratified fluids. The r.m.s. velocities and integral timescales were measured in these experiments, from which an integral lengthscale was calculated.

Hannoun *et al.* (1988) have shown that the turbulent quantities within the bulk of the patch (away from the interface) are independent of the stratification; near the interface, the horizontal turbulent velocity becomes proportional to its non-stratified counterpart.

In the stratified experiments, the tank was filled with a linearly stratified salt solution by employing the standard technique of Oster & Yamamoto (1963). The initial density profile was measured by a traversing conductivity probe and the background buoyancy frequency was calculated from

$$N_0^2 = -\frac{g}{\rho_0}\frac{\mathrm{d}\rho(z)}{\mathrm{d}z}, \tag{1}$$

where ρ_0 is the reference density, ρ is the density at a given height measured from the mean position of the grid, g is the acceleration due to gravity, z is the vertical coordinate, and $\rho_0 = \rho(0)$; see figure 2(*b*). The value of N_0 was varied over 0.3–1.7 rad s^{-1}.

The experiments were started (at time $t = 0$) by initiating the grid oscillations. The instantaneous salinity profiles through the patch were obtained by shooting the conductivity probe through the patch and the density fluctuations within the patch were obtained using the stationary conductivity probe. Typically, the traversing probe passes through the patch in about 0.2 s.

With time the local mean-buoyancy gradient N^2 within the patch decreases and eventually becomes nearly zero. In such cases, however, a useful buoyancy gradient can be defined in terms of the Thorpe-ordered density profile $\rho_{\mathrm{T}}(z)$ within the patch, namely

$$N^2 = -\frac{g}{\rho_0}\frac{\mathrm{d}\rho_{\mathrm{T}}(z)}{\mathrm{d}z}. \tag{2}$$

The Thorpe-ordering procedure essentially consists of the rearrangement of a measured density profile, which contains inversions, into a monotonically varying stable density profile known as the Thorpe-ordered density profile. The vertical distance (positive downwards) over which a fluid particle has to be displaced to achieve its position in the Thorpe-ordered profile is called the Thorpe displacement d_i. Since internal waves do not contain inversions (Phillips 1977), the Thorpe displacements are relatively free from effects owing to density perturbations associated with internal gravity waves. In calculating N^2, the instantaneous buoyancy profile was Thorpe-ordered using a standard bubble-sort routine and the least-square estimate of the mean buoyancy gradient over the patch was taken.

If the measured profile has distinct density values at sampling points (heights), then both the Thorpe-ordered profile and the Thorpe displacements are unique. A problem arises, however, when two or more points have the same density. In such cases the minimum distance required to bring each sample to the stable profile was considered as d_1. The Thorpe lengthscale L_{T} is defined as the r.m.s. value of the Thorpe displacements (Thorpe 1977; Dillon 1982), i.e.

$$L_{\mathrm{T}} = \left[\frac{1}{n}\sum_{i=1}^{n} d_i^2\right]^{\frac{1}{2}} \tag{3}$$

where n is the number of sampling points. Another scale that is used to represent the size of overturning eddies is the maximum Thorpe displacement. It is defined as,

$$(L_{\mathrm{T}})_{\max} = \max\{|d_i|\} \quad (i = 1, 2, \ldots, n). \tag{4}$$

The scales L_T and $(L_T)_{max}$ were calculated using (3) and (4) and the minimum distance between the points beyond with $|d_i| < 0.05(L_T)_{max}$ was defined as the thickness of the patch L_p.

A question arises, however, as to which buoyancy frequency is important in the dynamics of the patch. If the eddies are away from the patch boundaries, they do not sense the ambient stratification N_0 and their motions are governed by N. On the other hand, if the eddies interact with the ambient fluid, for example, by scouring heavy/light fluid particles, then the interfacial buoyancy jump, and hence N_0, is an important parameter. According to Caldwell (1983), for oceanic turbulent patches, the effective buoyancy gradient can be estimated by calculating the mean buoyancy gradient over a region somewhat larger than the estimated patch size. For the present case, however, there is a well-defined boundary between the ambient fluid and the patch; thus N_0 was used to parameterize the cases that involve the destruction of the ambient stratification, such as the growth of the patch, and for cases where eddy-motions within the patch are of interest, N was used as the significant parameter.

3. Measurement of grid-generated turbulence

Since the turbulent patch of the present experiments is energized by an oscillating grid, it is instructive to investigate the properties of grid-generated turbulence. Oscillating-grid turbulence is one of the well-studied cases of shear-free turbulent flows (see Hannoun *et al.* (1988) and references therein) and indeed this is the reason for selecting such a configuration for the present studies. Theoretical arguments of Long (1978*a*) show that, at high Reynolds numbers, the shear-free turbulence-producing properties of an oscillating grid can be represented by a single parameter called 'Action', defined as $K = u_H z$, where u_H is the r.m.s. horizontal velocity at a distance z from the grid plane. Long's predictions were found to be in agreement with a large number of earlier experimental studies performed using oscillating-grid turbulence. Of particular interest to the present experiments are the studies of Thompson & Turner (1975) and Hopfinger & Toly (1976). The grid parameters for these experiments were: $M = 5$ cm, $S = 1$ cm, $M/d = 5$, $f = 1.4$–6 Hz; and $M = 5$, 10 cm, $S = 4$, 8, 9 cm, $M/d = 5$, $f = 2$–6 Hz, respectively. Hopfinger & Toly proposed that oscillating-grid turbulence data can be fitted into the empirical power law of the form

$$u_H = B_1(S^3M)^{\frac{1}{2}}fz^{-1}, \tag{5}$$

$$w_H = B_2(S^3M)^{\frac{1}{2}}fz^{-1}, \tag{6}$$

$$l_H = B_3 z, \tag{7}$$

where $B_1, B_2 \ldots$ are constants for a given grid geometry (which may also have some dependence on the stroke), w_H is the r.m.s. vertical velocity, and l_H is the integral lengthscale of turbulence. Subscript H is used to denote the measurements in homogeneous fluids. Note that (5) can be used to calculate the action parameter as

$$K = u_H z = B_1(S^3M)^{\frac{1}{2}}f. \tag{8}$$

In this paper, K will be used to represent the grid as a turbulent energy source. Such a parameterization has a particular advantage in that it drastically reduces the number of non-dimensional parameters for the problem. Although K has been successfully used in some previous studies (Folse, Cox & Schexnayder 1981; Hopfinger & Linden 1982; Fernando & Long 1983, 1985*a*, *b*: E & Hopfinger 1986), it was felt that corroboration of (5)–(7) via direct measurement is useful in the

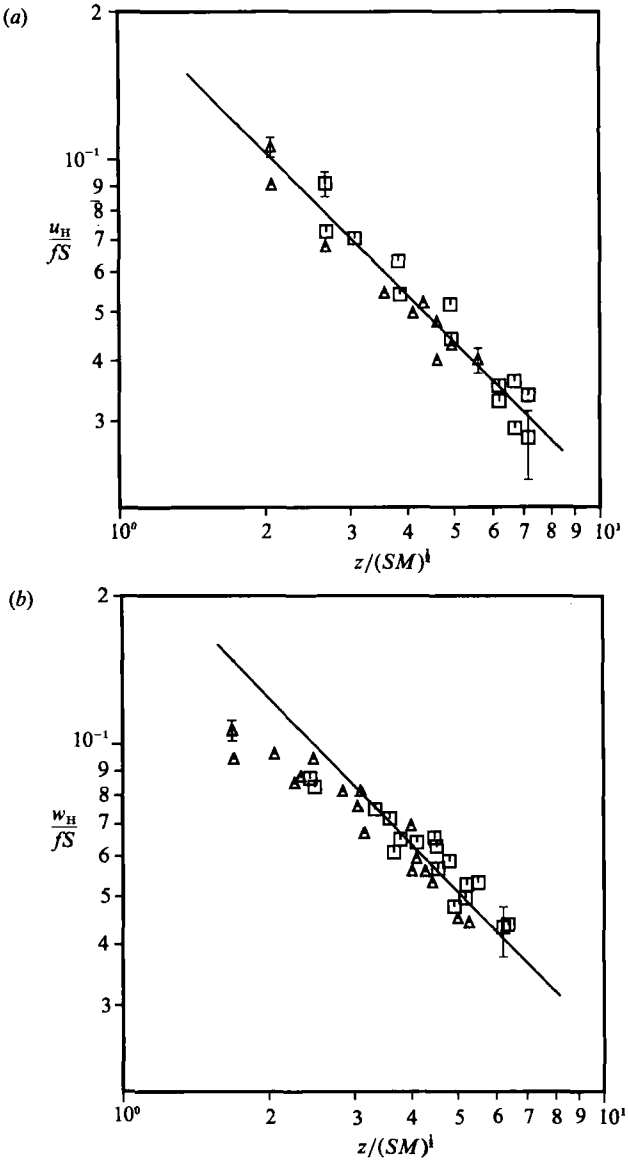

FIGURE 3. Measurements of (*a*) horizontal u_H and (*b*) vertical w_H r.m.s. velocities of grid-induced turbulence in homogeneous fluids. The data have been normalized according to (5)–(6). A grid with $M = 4.76$ cm was used in conjunction with strokes △, 2.1 cm and □, 0.85 cm.

present context. The results of these measurements are discussed below. The experiments on velocity measurements were carried out using the two grids having solidities of 36% ($M = 4.76$ cm, $M/d = 5.28$) and 50% ($M = 2.93$ cm, $M/d = 3.24$). The selection was based on a finding of Corrsin (1963) that jets and wake structure behind grid bars becomes unstable at solidities over 40%, whence the wakes deflect their axes and merge to form a larger wake structure. Secondary circulations and strong inhomogeneities are bound to be generated in such situations. When the solidity is smaller than 40%, the wakes coalesce with each other without bending their axes; shear-free turbulence can be expected on either side of the grid at sufficiently large z.

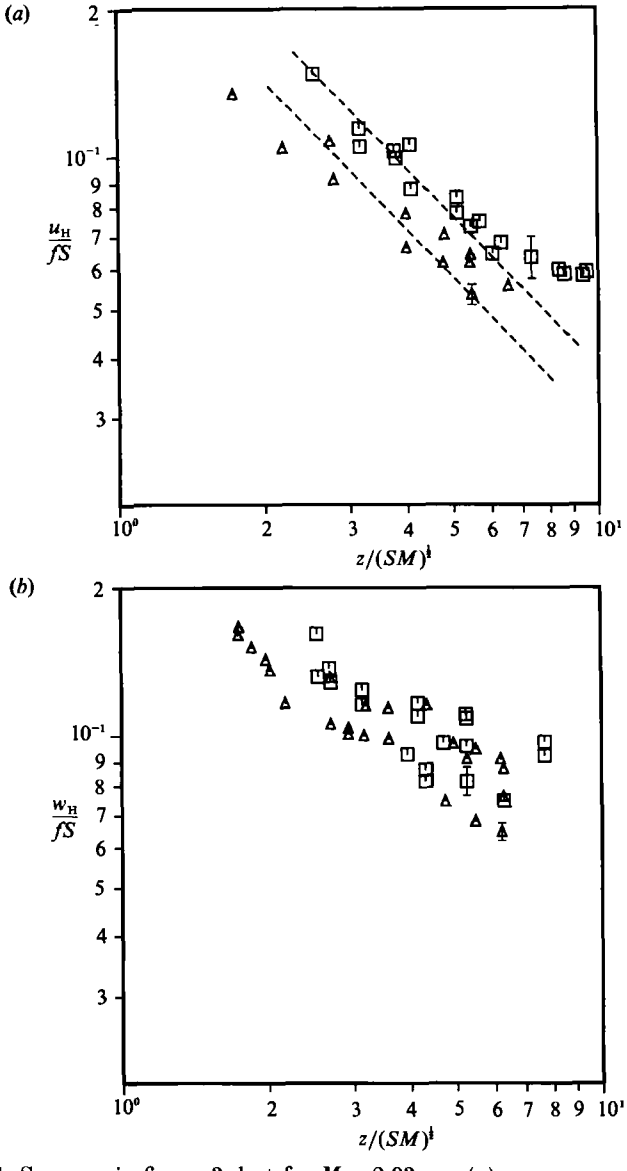

FIGURE 4. Same as in figure 3, but for $M = 2.93$ cm. (*a*) ———, eye-fitted -1 slopes for the data.

Velocity measurements pertinent to $M = 4.76$ cm grid are shown in figure 3 for two different strokes $S = 0.85$ cm and 2.1 cm. For a given z, measurements were made at five horizontal positions (according to McDougall's (1979) selection of measurement points) and the average was taken. The horizontal and vertical velocity data have been plotted in accordance with (5) and (6); the agreement appears to be satisfactory, particularly when $z/(SM)^{\frac{1}{2}} > 3$. The measured values of $B_1 \approx 0.22$ and $B_2 \approx 0.26$ compare very favourably with those of Hopfinger & Toly (1976) who found $B_1 \approx 0.25$ and $B_2 \approx 0.27$. On the other hand, experiments performed with the grid of high solidity ($M = 2.93$ cm) did not agree with (6) (see figure 4). This is not surprising in view of possible wake merging and large-scale inhomogeneities present in such situations. Thus, it is concluded that the concept of grid action can be employed only at low solidities.

The integral lengthscale could not be directly measured and was calculated using the integral timescale τ based on the temporal autocorrelation function. The calculated lengthscale $l = u_H \tau$ was compared with (7) for the case of $M = 4.76$ cm and B_3 was found to be 0.1. One of the concerns in these experiments was the effect of grid-induced flow near the grid. The sizes of the patches vary from about 4 cm to 20 cm, and it was necessary to determine whether the interfacial fluid motions are affected by this forced flow. The mean velocity was calculated from velocity traces obtained at different z, for different f. The results show that for $f < 4$ Hz, the grid does not produce significant forced flow at $z > 4$ cm. This was confirmed by calculating the energy (frequency) spectra, which show a 'hump' near f if the forced motion is significant. Thus, patches of size $L_p > 8$ cm can be considered as free from unwarranted grid-effects.

4. Experiments with density stratification

4.1. *Mixing within the patch*

Qualitative observations made during the patch growth were in agreement with the observations of Fernando (1988) discussed in §1. Initially the patch size grew as $L_p \propto (Kt)^{\frac{1}{2}}$, until a time $N_0 t_c \approx 4$ where its growth is retarded by buoyancy effects. At large times the patch grows slowly via breaking of interfacial waves. A set of density profiles taken during the evolution of the patch is shown in figure 5, in which the destruction of the density gradient and the presence of small-scale inversions owing to stirring are evident. Turbulence destroys the initial stable stratification, entrains non-turbulent fluid into the patch and mixes it with the rest of the fluid. At small $N_0 t$ values, all of the above processes are important, whereas, at large $N_0 t$, the initial stratification within the patch has already been destroyed and the entrainment makes the dominant contribution to the inversions. As illustrated in figure 1 (*b*), entrainment at large $N_0 t$ occurs by the intermittent breaking of interfacial waves, during which secondary mixed regions of density intermediate to that of the interfacial layer and the mixed layer are produced and merge with the mixed layer (also see figure 6). As these fluid lumps enter the mixed layer, they are broken up by different-sized eddies and are redistributed. According to Pearson, Puttock & Hunt (1983), such newly-arrived fluid lumps lose their identity and homogenize with the rest of the fluid at a time βN^{-1}, where $\beta \approx 5$ (Hunt, Kaimal & Gaynor 1985).

It is possible to quantify the degree of mixing within the patch by introducing a 'mixedness' parameter γ, defined as

$$\gamma = 1 - \frac{N^2}{N_0^2}, \tag{9}$$

where N is defined by (2). Note that γ typifies the degree of destruction of the initial stratification as well as the buoyancy contributions due to entrainment. On physical grounds, it is reasonable to expect γ to depend on N_0, the nature of the turbulence source (K), and the time of agitation t, namely

$$\gamma = f_1(K, t, N_0), \tag{10}$$

where $f_1, f_2 \ldots$ are used to denote functions. Further, the patch size L_p is a function of the same parameters, so that it is possible to eliminate N_0 in (10) as

$$\gamma = f_2\left(\frac{Kt}{L_p^2}\right). \tag{11}$$

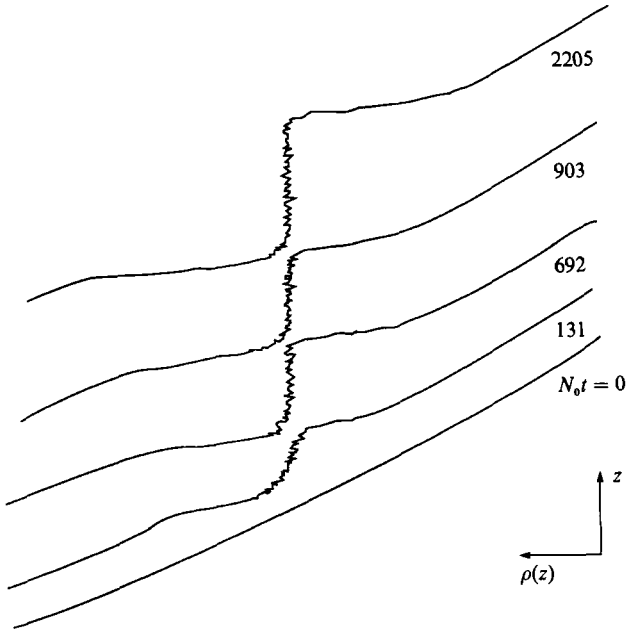

FIGURE 5. Density profiles taken through a growing patch at different non-dimensional times.

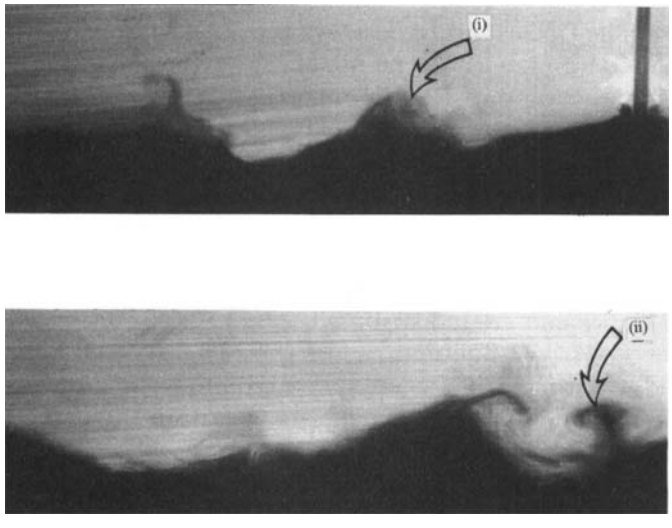

FIGURE 6. Photographs of the interface which show wave breaking: (i) appearance of a wave breaking event; (ii) release of a dense fluid parcel into the turbulent layer during an interfacial wave-breaking event.

Figure 7 shows the variation of γ with Kt/L_p^2 for several experiments, where N values were calculated using Thorpe-ordered density profiles. Note that γ initially increases rapidly and then levels off after about $Kt/L_p^2 \approx 5$, corresponding to $N_0 t \approx 400$, whence $\gamma \approx 0.9$. When the patch growth is first arrested by the stratification at $N_0 t_c \approx 4$, $Kt/L_p^2 \approx 0.2$ and thus figure 7 does not include data from the initial growth regime. The initial growth lasts only for a short time ($N_0 t < 4$) and it is difficult to obtain an extensive set of profiles through the patch within that time frame.

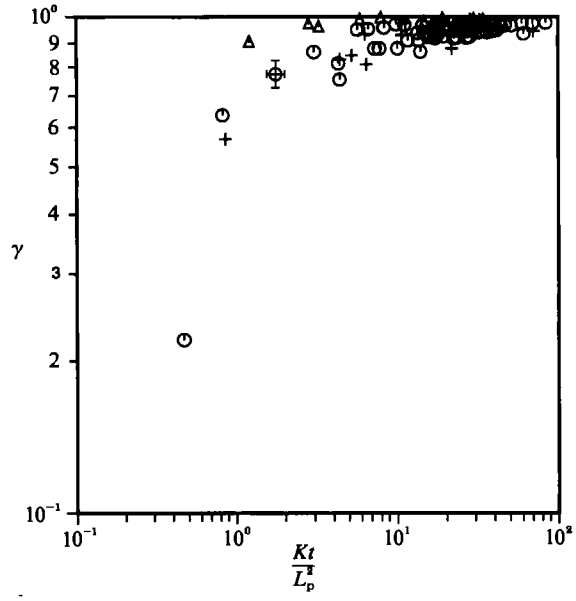

FIGURE 7. Variation of the 'mixedness' γ of the patch with the parameter (Kt/L_p^2). ○, $M = 4.76$ cm; +, 6.20 cm; △, 2.93 cm.

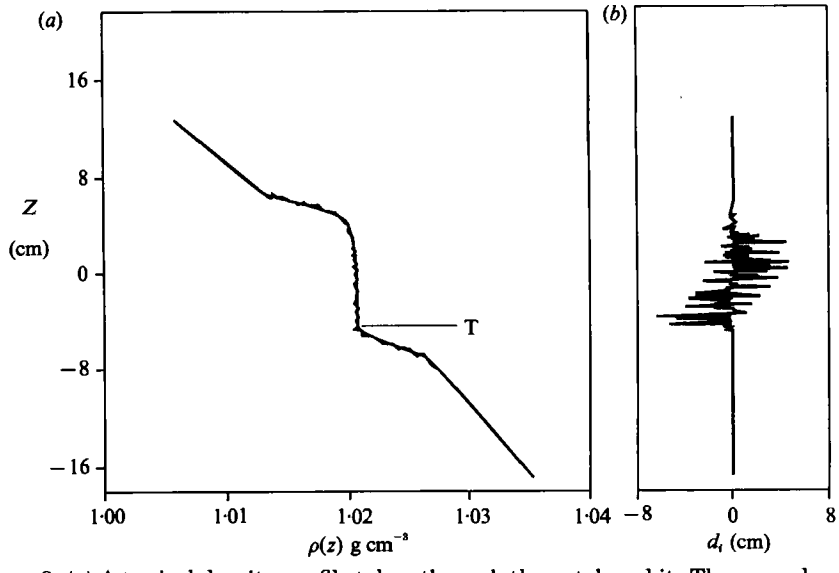

FIGURE 8. (*a*) A typical density profile taken through the patch and its Thorpe-ordered counterpart (designated as T). (*b*) The Thorpe displacement diagram of the density profile given in (*a*).

Data taken using all three grid sizes are shown. Note that the data taken using the grids with solidity less than 40% ($M = 6.20$ cm and 4.76 cm) show the same trend whereas the data corresponding to the grid with solidity greater than 40% ($M = 2.93$ cm) consistently showed somewhat higher γ. Apparently γ never reaches unity owing to the fact that fluid entrainment due to wave breaking generates a small mean density gradient (in the Thorpe-ordered sense) within the mixed layer.

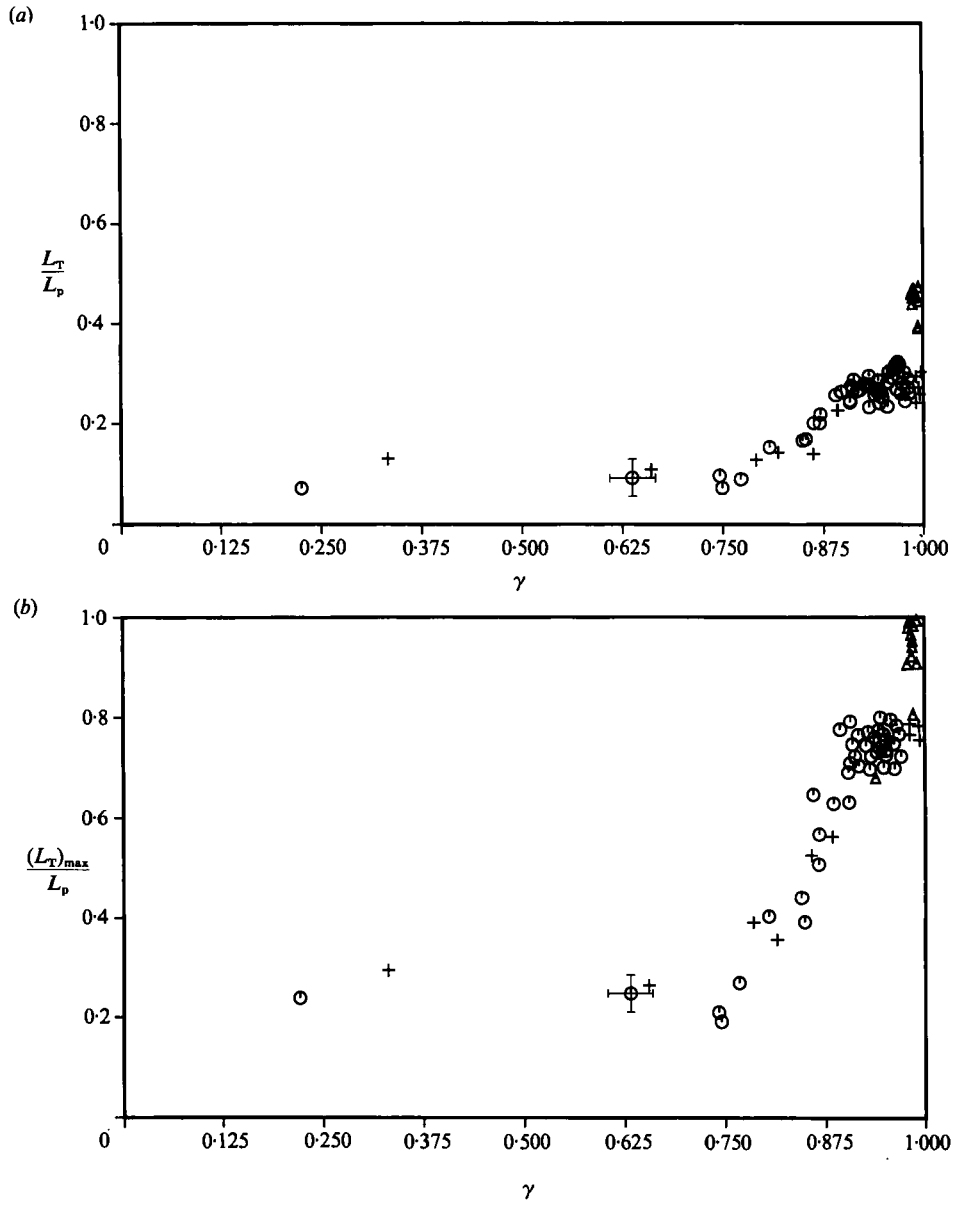

FIGURE 9. Variation of (a) L_T/L_p and $(L_T)_{max}/L_p$ with γ.

4.2. *Measurements of Thorpe lengthscale*

Using the same arguments as were used in deriving (10) and (11), it is possible to write

$$L_T/L_p = f_3(\gamma), \tag{12}$$

$$(L_T)_{max}/L_p = f_4(\gamma). \tag{13}$$

In order to compare (12) and (13) with the experimental results, the instantaneous density profiles were Thorpe-ordered by sorting and rearranging the array of measured density values into a statically stable distribution (§2). A representative density profile, its Thorpe-ordered counterpart, and the corresponding Thorpe

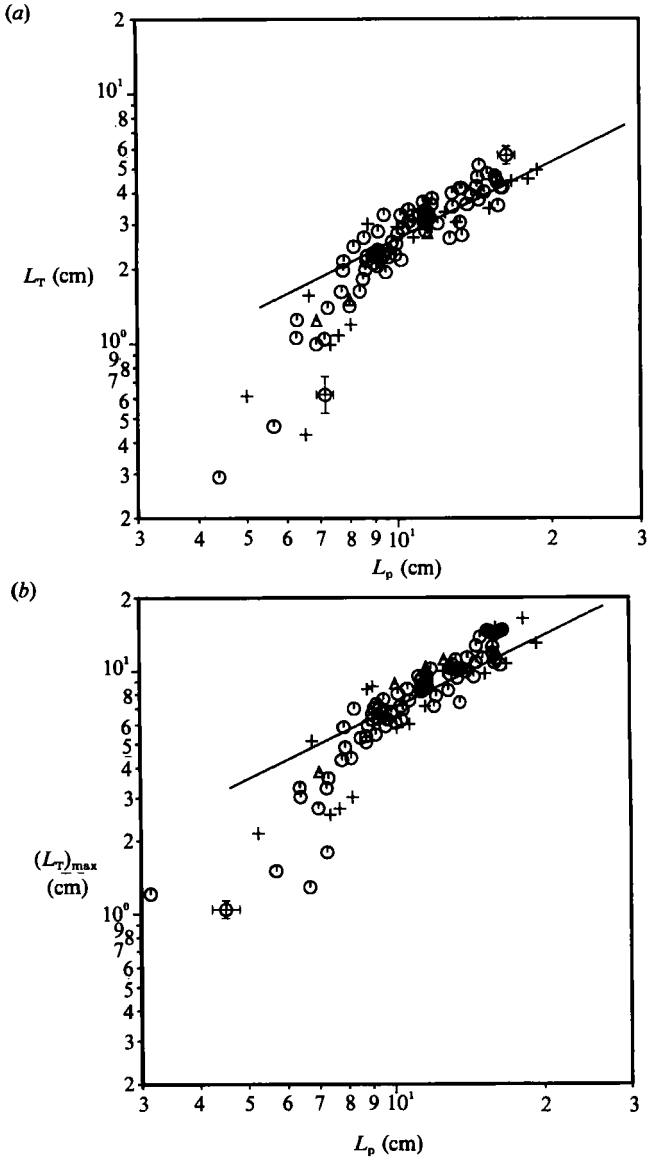

FIGURE 10. Variation of (*a*) L_T and (*b*) $(L_T)_{max}$, with L_p when $N_0 t > 400$.

displacements are shown in figure 8. This clearly shows that the Thorpe displacements, which characterize the inversions, occur only within the patch. Sometimes it was found that the Thorpe-ordered density distribution is not linear although the initial density distribution is linear.

The variations of L_T/L_p and $(L_T)_{max}/L_p$ with γ are shown in figure 9 for experiments carried out with all three grids. For clarity, only a few points taken for the grid with $M = 2.93$ cm at large γ are shown. Note that for the cases $M = 4.76$ cm and 6.20 cm, both L_T/L_p and $(L_T)_{max}/L_p$ increase sharply in the range $0.7 < \gamma < 0.9$ and then level off. A correlation analysis performed using the data for $\gamma > 0.9$ (or $N_0 t > 400$) shows that L_T/L_p and $(L_T)_{max}/L_p$ are essentially independent of γ. For the grid $M = 2.93$ cm, the data are scattered and did not show a particular trend. Thus

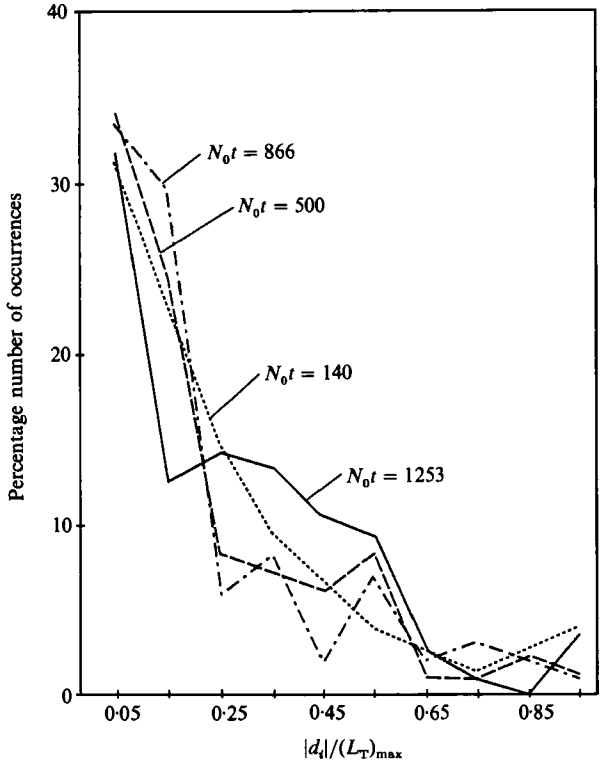

FIGURE 11. Distribution of fluid particle displacements for four different conductivity probe traverses through the patch: $N_0 = 1.21$ rad s^{-1}; $K = 1.43$ cm^2 s^{-1}.

henceforth, unless otherwise stated, only the data taken with $M = 4.76$ cm and 6.20 cm are presented, and they are represented by symbols ○ and +, respectively.

Figure 10 shows the variation of L_T and $(L_T)_{max}$ with L_p, when $\gamma > 0.9$ or $N_0 t > 400$. Note that for $L_p > 8$ cm, linear dependencies between L_T, $(L_T)_{max}$ and L_p are evident. The best fit lines with +1 slope drawn from the data at $L_p > 8$ cm suggest the relations

$$L_T \approx 0.27 L_p, \quad (L_T)_{max} \approx 0.74 L_p. \tag{14}$$

The estimated errors are shown using error bars. The departure of the data from (14) at $L_p < 8$ cm can be attributed to the presence of grid-induced forced flow near the interface, as discussed in §3.

Gibson (1987) has used what is called a 'slotted z model' to calculate the Thorpe displacements in a stratified turbulent patch. The model is valid for the period of initial mixing, in which the buoyancy gradient is destroyed, and predicts $L_T = 0.41 L_p$. The present results, however, show that during the initial mixing, L_T/L_p is a function of γ and, after $N_0 t > 400$, $L_T \approx 0.27 L_p$. It is interesting to note that the relation $(L_T)_{max}/L_T \approx 2.74$, resulting from (14), is the same as that found by Itsweire (1984) during decaying stratified turbulence experiments. This result suggests that the characteristics of Thorpe scales and maximum Thorpe displacements can be the same whether the turbulence is decaying or sustained.

The occurrence of a given (normalized) Thorpe displacement $|d_i|/(L_T)_{max}$ as a percentage of total Thorpe displacements is shown in figure 11; distributions corresponding to four density profiles are shown. Although the details vary, these

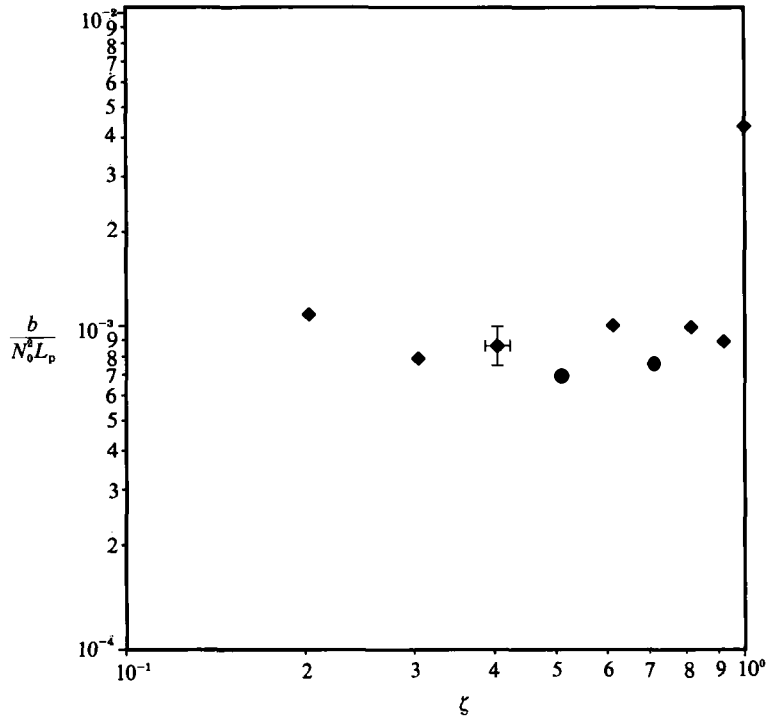

FIGURE 12. Spatial variation of the normalized r.m.s. buoyancy fluctuation $b/N_0^2 L_p$ within the patch.

distributions indicate the general trend that small-scale overturning events that displace fluid particles over much shorter distances compared to the size of the patch prevail.

4.3. *Measurement of overturning lengthscale* L_t

The dominant eddy overturning lengthscale (sometimes called the Ellison scale or turbulent scale) is defined as

$$L_t = \frac{b}{N^2}, \tag{15}$$

where b is the r.m.s. buoyancy fluctuation. It is commonly used in stratified turbulence studies as an indicator of the size of the largest overturning eddies. Since b is an Eulerian measurement, in general L_t contains spatial and/or temporal influences of both internal waves and turbulence at the measurement point; hence it does not offer useful information on the overturning motions. Later works have offered minors corrections to the definition of L_t. For example, in conjunction with their solid-body rotation model, Stillinger, Helland & Van Atta (1983) proposed that L_t should be defined as $2b/N^2$ whereas Gargett, Osborn & Nasmyth (1984) have shown that the definition $2\sqrt{2}b/N^2$ is more consistent with the solid-body rotation model.

Since the patch can be considered as quasi-stationary only when $N_0 t > 400$ or $\gamma > 0.9$, b within the patch was measured only at $N_0 t > 400$. Figure 12 shows the spatial variation of b within the patch, where $\zeta = 2z/L_p$. The buoyancy jump across the patch $N_0^2 L_p$ has been used to normalize b. Within the patch b appears to be constant and its sudden increase at the edge of the patch is due to the interfacial

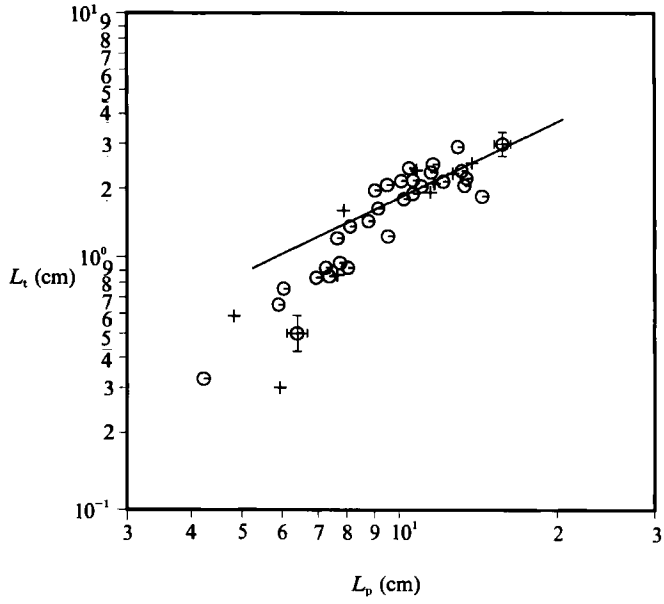

FIGURE 13. A plot of L_t *vs.* L_p; measurements have been taken at $N_0 t > 400$.

waves. In calculating L_t, b corresponding to $z = \frac{1}{4}L_p$ was used; the results are shown in figure 13. Note that, for $L_p > 8$ cm, a relationship of the form

$$L_t = 0.18 L_p, \tag{16}$$

can be discerned, independent of the grid parameters. Note that the measurements were made in a well-mixed ($\gamma > 0.9$) patch and the influence of internal waves can be considered to be minimal.

4.4. *Measurement of buoyancy lengthscale* L_b

The buoyancy lengthscale is defined as

$$L_b = \frac{w}{N}, \tag{17}$$

where w is the r.m.s. vertical velocity. As in the case of L_t, L_b is also sensitive to both turbulence and internal waves. It represents the maximum vertical distance that a fluid particle travels from its equilibrium position before its initial vertical kinetic energy is fully expended by the increase of its potential energy (Long 1978*b*) or until the vertical inertia and buoyancy forces balance each other (Gibson 1980). In reality, however, only a fraction of the vertical kinetic energy can be converted into potential energy.

The initial growth of the patch can be interpreted as corresponding to a stage where the vertical inertia forces of energy-containing eddies ($w^2/l \sim K^2/L_p^3$) vastly exceed the buoyancy forces associated with them ($N^2 l \sim N^2 L_p$); here l is the size of the energy-containing eddies. As the patch grows, this force imbalance gradually reduces and, at a certain critical patch size $(L_p)_c$, a force balance is expected. Using the given parameterizations, it is possible to estimate $(L_p)_c \sim (l)_c \sim (L_b)_c$, where the subscript c denotes the critical conditions. Before the buoyancy forces become important, the stratification has a negligible effect on turbulence, and hence $(w)_c$ can be approximated as w_H of the source turbulence. An alternative explanation can be advanced by considering the superimposition of linear stratification and source

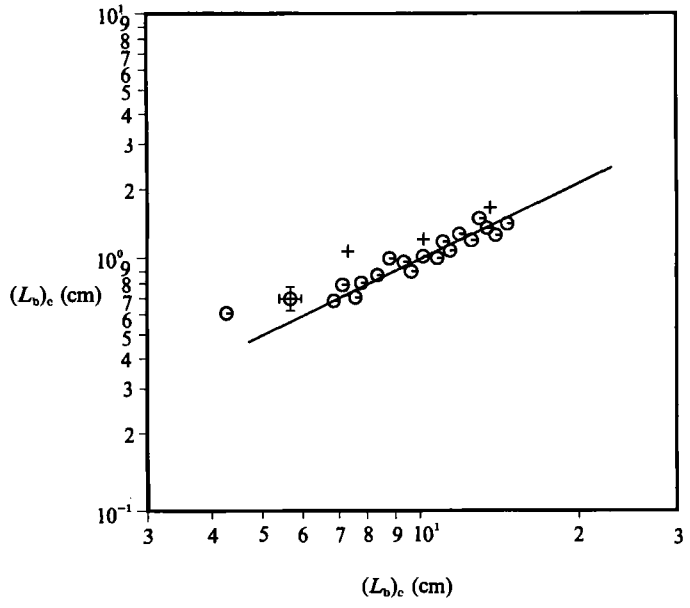

FIGURE 14. A plot of $(L_b)_c$ *vs.* $(L_p)_c$.

turbulence. Based on (6) and (7), the effective vertical inertia forces of the eddies can be expected to decay as K^2/z^3. If these eddies are to perform overturning motions against the stratification, the buoyancy forces to be overcome should be of the order N^2z. Thus, the fluid particles lying at distances beyond $z \sim w_H/N = L_b$ cannot be mixed turbulently (but can sustain wave motions), and the turbulence is confined to a patch of size $(L_p)_c \sim L_b$.

Figure 14 shows the variation of L_b and L_p under critical conditions. In calculating $(L_b)_c$, w_H corresponding to the interfacial position was used. The proportionality between $(L_b)_c$ and $(L_p)_c$ indicates support for the scaling arguments discussed above. The straight line indicates,

$$(L_b)_c \approx 0.1(L_p)_c. \tag{18}$$

Another commonly used lengthscale is the Ozmidov (1965) lengthscale. It is defined as

$$L_R = \left[\frac{\epsilon}{N^3}\right]^{\frac{1}{2}}, \tag{19}$$

where ϵ is the rate of dissipation of turbulent kinetic energy. If it is assumed that ϵ can be parameterized as $\epsilon = Cw^3/l$, where C is a constant, it is possible to obtain $L_R l^{\frac{1}{2}} \sim L_b^{\frac{3}{2}}$. At the critical conditions $l \sim L_b$, and hence $L_R \sim L_b$. In the present experiments, ϵ was not measured, but was calculated using the value $C \approx 0.61$ proposed by Hopfinger & Toly (1976). The results were found to follow the relation $(L_R)_c \approx 0.12(L_p)_c$.

The quantities L_t, L_b and L_R have been measured in stratified water and wind-tunnel experiments by Stillinger *et al.* (1983), Itsweire, Helland & Van Atta (1986), Lienhard & Van Atta (1990), and Yoon & Warhaft (1990). These experiments are different from the present work in the sense that small-scale decaying turbulence produced by a grid/mesh was superimposed on the stratification and the evolutions of the lengthscales were measured. The present experiments deal with a single isolated forced turbulent patch. The results of the wind/water tunnel experiments at the onset of buoyancy effects (critical conditions) are summarized below.

Stillinger *et al.* (1983):

$$L_t \approx 0.70 L_R, \quad L_R \approx 1.49 L_b^{1.53}, \tag{20}$$

Itsweire *et al.* (1986):

$$L_t \approx 0.85 L_R, \quad L_R \approx 1.31 L_b^{1.4}, \tag{21}$$

Lienhard & Van Atta (1990):

$$L_t \approx (0.15\text{–}0.17) L_R, \quad L_t \approx (0.30\text{–}0.34) L_b, \tag{22}$$

Yoon & Warhaft (1990):

$$L_b \approx (0.40\text{–}0.67) L_R, \quad L_t \approx 0.25 L_b. \tag{23}$$

The differences in the coefficients are usually attributed to the differences in the Prandtl numbers and the presence of a strong internal gravity wave field in salt-stratified experiments. Also note that the relationships between L_R and L_b given by Stillinger *et al.* and Itsweire *et al.* are valid even after the onset of buoyancy effects.

4.5. *Measurement of available potential energy of the fluctuations*

The potential-energy change due to the exchange of two particles of a Thorpe-ordered density profile is either positive if the particles have different densities, or zero if the densities of the particles are identical. Hence, the Thorpe-ordered profile can be considered as a state of minimum potential energy and it is useful to quantify the difference in potential energies of a given profile and its Thorpe-ordered counterpart. The available potential energy of the fluctuations, A, which is defined as (Dillon 1984)

$$A = \frac{g}{n\rho_0} \sum_{i=1}^{n} [\rho(z_i) - \rho_T(z_i)] z_i, \tag{24}$$

can be used for this purpose. Here $\rho_T(z_i)$ is the density distribution in the Thorpe-ordered density profile and $\rho(z_i)$ is the measured density at depth z_i. Note that A does not include potential-energy fluctuations due to internal wave motions since their contributions to the Thorpe displacements are negligible.

If the Thorpe-ordered profile within the patch is linear, then it is possible to show that (Crawford 1986; Dillon & Park 1987)

$$A = \tfrac{1}{2} L_T^2 N^2. \tag{25}$$

Figure 15 shows a plot of A versus $\frac{1}{2} L_T^2 N^2$ for the present experiments; data points taken at $N_0 t \gtrsim 400$ are included. For large A values, the experimental data are clustered around the line

$$A = \tfrac{1}{2}(1.17) L_T^2 N^2, \tag{26}$$

irrespective of the mesh sizes of the grid, indicating that the Thorpe profiles can be regarded as nearly linear. General observations show that nonlinearities of density profiles occur near the interfaces, and within the patch the density profile is approximately linear. At small A, the data clearly tend to deviate from (25) indicating the nonlinear nature of the Thorpe profiles.

4.6. *Growth characteristics of the patch*

The turbulent patch grows owing to the propagation of the front. On dimensional grounds it is easily shown that the growth of the patch should follow

$$\frac{L_p}{2(K/N_0)^{\frac{1}{2}}} = f_5(N_0 t), \tag{27}$$

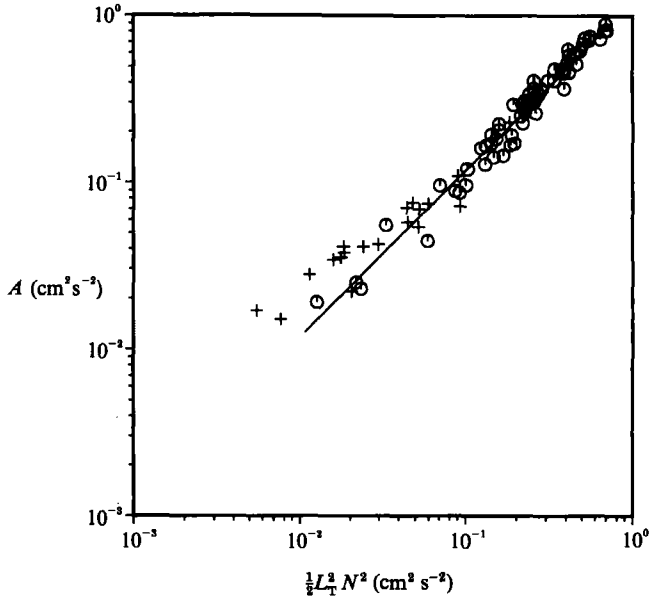

FIGURE 15. Variation of A with $\frac{1}{2}L_T^2N^2$. The line represents the best-fit line with slope 1 to the data at $\frac{1}{2}L_T^2N^2 > 0.1$, about which the bulk of the experimental points are clustered.

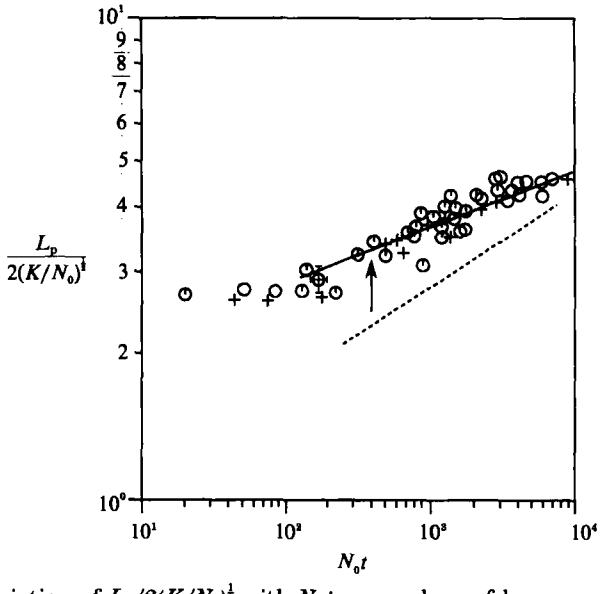

FIGURE 16. Variation of $L_p/2(K/N_0)^{\frac{1}{2}}$ with N_0t. ——, slope of $\frac{1}{8}$. ------, the trend of the collected data when a grid of mesh size $M = 2.93$ cm was used. The time $N_0t = 400$ is indicated by an arrow.

and, according to Fernando (1988), at $N_0t < 4$, $f_5 \sim (N_0t)^{\frac{1}{2}}$ and the buoyancy effects are unimportant in this regime. The present results corroborated this observation, although owing to the larger stroke they might have been contaminated by grid effects. At $N_0t = 4$, the patch growth is temporarily halted and, as is evident from figure 16, at large times the patch starts growing at a much slower rate. Shadowgraph observations clearly showed that the patch growth is symmetrical about the grid plane, thus corroborating the theoretical arguments of Redondo (1990). Note that

the patch growth is independent on grid parameters for $M = 4.76$ cm and 6.20 cm; the grid with high solidity ($M = 2.93$ cm), however, showed a widely different behaviour. The trend of the data for the latter case is shown by the dotted line on figure 16.

It is interesting to note that the subsequent growth of the patch is clearly evident at $N_0 t > 400$, or when $\gamma > 0.9$. Apparently, when $N_0 t < 400$, the energy supplied by the source is mainly used for the degradation of the buoyancy gradient within the patch, and the energy available for exciting the interfacial waves is negligible. Since the braking of such waves is responsible for subsequent growth, only at large $N_0 t$ values it is possible to expect an appreciable growth. Further, note that the subsequent growth law of the patch follows $L_p/2(K/N_0)^{\frac{1}{2}} \sim (N_0 t)^{\frac{1}{8}}$, which is the same as $u_e/u_H \sim Ri^{-\frac{3}{2}}$ (Fernando 1988), where u_e is the propagation speeds of the interfaces, Ri is the Richardson number $Ri = \Delta b l_H/u_H^2$ and Δb is the buoyancy jump across the interface. This is the same as the entrainment law observed during the propagation of a single interface by E & Hopfinger (1986). Thus, the results show that the interfaces propagate independently of each other as in the previous mixed-layer deepening experiments when the stratification in the patch was nearly destroyed.

4.7. *Properties of interfacial waves*

Communication of the turbulent motions of the patch with the ambient stratification can occur through the radiation of internal waves via the interfacial layer (Carruthers & Hunt 1986). Fernando & Long (1985*b*), however, have argued that the interfacial layer can act as a sink of internal-wave energy, in that the waves are trapped within the layer and dissipate energy by breaking; this process leaves an insufficient amount of wave energy at the outer edge of the interfacial layer to be radiated outwards. In the present study, a conductivity probe was positioned in the lower stratified layer, 1.5 cm away from the interface, and the buoyancy fluctuations were recorded continuously to detect any generation of internal waves. No significant wave generation was observed. The measurements of dominant wave amplitudes and frequencies at the entrainment interface have been performed by Fernando (1988) and the results show that under critical conditions, they are proportional to $(L_p)_c$ and N_0, respectively. In the present study, the buoyancy fluctuations were measured at the mid-point of the interfacial layer. A typical frequency spectrum $\psi(\omega)$ obtained in this way is shown in figure 17.

A form of $\psi(\omega)$ can be obtained by assuming that interfacial waves are generated by interfacial distortions that result from the eddy impingement on the interface. If it is assumed that different sizes of eddies of scales smaller than $l \sim l_H$ are advected over the interface by the energy-containing eddies, the frequency of the disturbances caused by an eddy of wavenumber k (in an Eulerian sense) is given by (Tennekes & Lumley 1973)

$$\omega \sim uk \sim u_H k, \tag{28}$$

and the associated velocity fluctuation can be written as

$$w_\omega \sim (\epsilon k^{-1})^{\frac{1}{3}}. \tag{29}$$

Upon impingement on the interface, such eddies will cause an interfacial distortion δ_ω, determined by a balance between vertical kinetic energy of the eddies and the potential energy stored owing to the distortion, i.e.

$$\delta_\omega \sim \frac{w_\omega}{N_0}. \tag{30}$$

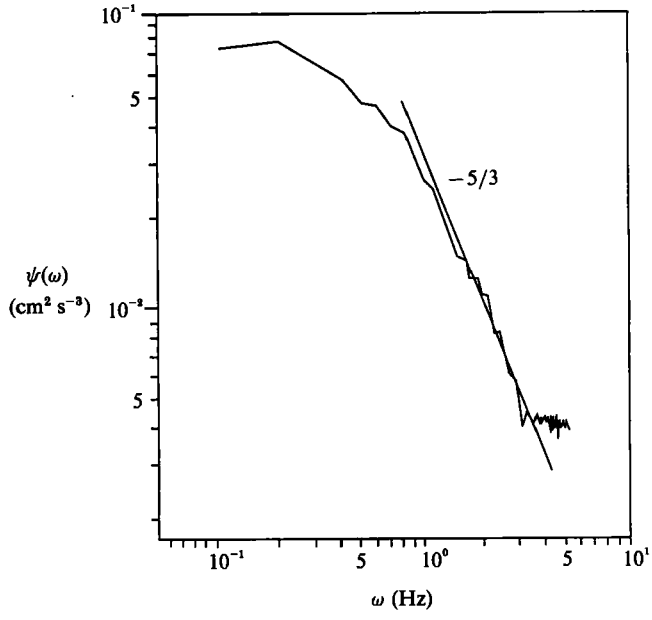

FIGURE 17. A frequency spectrum $\psi(\omega)$ of buoyancy fluctuations measured at the mid-point of the density interface. The experimental conditions are $K = 1.72$ cm^2 s^{-1}; $N_0 = 1.12$ rad s^{-1}; $z = 7.6$ cm. The solid line has a slope of $-\frac{5}{3}$.

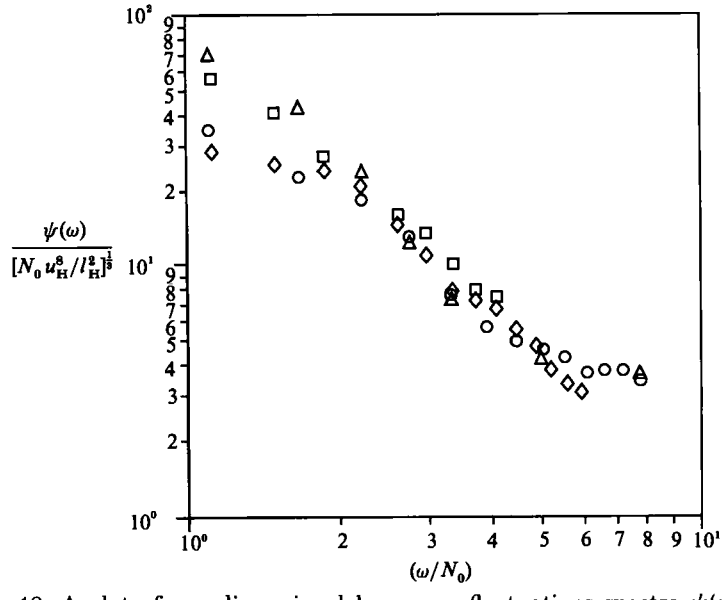

FIGURE 18. A plot of non-dimensional buoyancy fluctuations spectra $\psi(\omega)/(N_0 u_H^8/l_H^2)^{\frac{1}{3}}$ *vs.* non-dimensional frequency (ω/N_0). ◇, $N_0 = 1.67$ rad s^{-1}, $K = 1.80$ cm^2 s^{-1}, $z = 6.5$ cm; △, $N_0 = 1.12$ rad s^{-1}, $K = 1.77$ cm^2 s^{-1}, $z = 11.6$ cm; ○, $N_0 = 1.67$ rad s^{-1}, $K = 1.83$ cm^2 s^{-1}, $z = 10.3$ cm; □, $N_0 = 1.12$ rad s^{-1}, $K = 1.77$ cm^2 s^{-1}, $z = 10.8$ cm.

The corresponding fluctuation of buoyancy b_ω can be written as

$$b_\omega \sim N_0^2 \delta_\omega. \tag{31}$$

Using (28)–(31), together with $\epsilon \sim u_{\mathrm{H}}^3/l_{\mathrm{H}}$, it is possible to write,

$$b_\omega^2 \sim N_0^2 \left[\frac{u_{\mathrm{H}}^4}{\omega l_{\mathrm{H}}}\right]^{\frac{2}{3}}. \tag{32}$$

Thus, the spectra for buoyancy fluctuations becomes

$$\psi(\omega) \sim N_0^2 \left[\frac{u_{\mathrm{H}}^4}{l_{\mathrm{H}}}\right]^{\frac{2}{3}} \omega^{-\frac{5}{3}}, \tag{33}$$

or

$$\frac{\psi(\omega)}{\left[\dfrac{N_0 u_{\mathrm{H}}^8}{l_{\mathrm{H}}^2}\right]^{\frac{1}{3}}} \sim \left(\frac{\omega}{N_0}\right)^{-\frac{5}{3}}, \tag{34}$$

where (34) is valid for wave disturbances generated by eddies of sizes smaller than l or for $\omega > u_{\mathrm{H}}/l_{\mathrm{H}}$. Figure 18 shows a plot of $\psi(\omega)/(N_0 u_{\mathrm{H}}^8/l_{\mathrm{H}}^2)^{\frac{1}{3}}$ versus the non-dimensional frequency (ω/N_0). The proposed scaling collapses the frequency spectra for different experiments satisfactory.

5. Summary and discussion

The objective of the present study was to investigate turbulent mixing and overturning motions within a stratified turbulent patch that is continuously forced by an external source of turbulence. The salient findings of the present study are listed below:

(i) The generation of turbulence within a linearly stratified fluid develops a mixed layer which grows, as in a non-stratified fluid, for a time period of $t_{\mathrm{c}} \approx 4N_0^{-1}$ (initial growth). At $t = t_{\mathrm{c}}$, the growth is arrested by buoyancy effects, whence the following lengthscale relationships are valid.

$$L_{\mathrm{p}} \approx 20 l_{\mathrm{H}} \approx 5.6 L_{\mathrm{t}} \approx 10 L_{\mathrm{b}},$$

where L_{p} is the patch size, and l_{H}, L_{t} and L_{b} are integral scale of source turbulence, overturning lengthscale and buoyancy lengthscale, respectively. The Ozmidov lengthscale L_{R} was also calculated by estimating the rate of turbulent kinetic energy dissipation within the patch, and the relationship $L_{\mathrm{R}} \approx 0.12 L_{\mathrm{p}}$ was obtained for the conditions at $t = t_{\mathrm{c}}$.

(ii) The growth at $t > t_{\mathrm{c}}$ occurs slowly by breaking of the internal gravity waves generated at the entrainment interface. These waves are trapped within the interfacial layer and break by saturation. The internal wave energy radiated outwards into the ambient stratification was found to be negligible. The spectrum of the interfacial buoyancy fluctuations scales with $(N_0 u_{\mathrm{H}}^8/l_{\mathrm{H}}^2)^{\frac{1}{3}}$, when ω is scaled with N_0.

(iii) The subsequent growth of the patch becomes prominent at times $N_0 t \gtrsim 400$ or when $\gamma > 0.9$. This is consistent with the fact that at such times the density gradient within the patch is nearly destroyed and the energy input by the source can be used to generate internal waves at the interface. The growth approximately follows the power law $L_{\mathrm{p}}/2\,(K/N_0)^{\frac{1}{2}} \sim (N_0 t)^{\frac{1}{3}}$, indicating that the interfaces propagated independently as if one or the other was not present.

(iv) The Thorpe lengthscale within a patch is a function of both L_p and the *mixedness* γ of the patch. However, when $\gamma > 0.9$ the following relations hold.

$$L_T \approx 0.27 L_p,$$

$$(L_T)_{max} \approx 0.74 L_p.$$

(v) The rate of decrease of the average density gradient of the Thorpe-ordered profile is very small at large times. The newly arriving fluid particles due to interfacial wave-breaking tend to maintain a weak density gradient even at $N_0 t > 2000$.

(vi) The bulk of the available potential energy fluctuations data cluster around the line $A = 0.59 L_T^2 N^2$. According to oceanic observations of Crawford (1986) and Dillon & Park (1987), the proportionality constant between A and $\frac{1}{2} L_T^2 N^2$ can vary by a factor of 2 to 3, depending on the nonlinearity of the Thorpe profile.

(vii) Examination of the magnitudes of the Thorpe displacements suggests that most of the overturning motions displace fluid particles over short distances. For instance, the occurrence of Thorpe displacements greater than $0.9(L_T)_{max}$ is less than about 4%.

Although the intention of the present study was to obtain information that is useful in modelling various geophysical-flow situations, it should be noted that, at least in the oceanic context, the exact nature and strength of turbulence sources are not known and the extrapolation of the laboratory results to oceanic cases should be done with caution.

Commonly quoted oceanic-turbulence-generating mechanisms are internal wave breaking, shear-flow instabilities such as Kelvin–Helmholtz billowing, flow past obstacles such as sea mounts and guyots, double diffusion and critical-layer absorption. Turbulence thus generated differs greatly from the oscillating-grid induced turbulence. Gibson (1980) has argued that oceanic turbulent patches are a result of powerful short-lived turbulence-generating events ('big bangs'), and the patches are usually in a 'fossilized state' during the observation; fossil turbulence is defined as 'remnant fluctuations in some hydrophysical fields which persist after the fluid has ceased to be turbulent at the scale of the fluctuations'. A contrasting notion, called the 'continuous-creation hypothesis' has been proposed by Caldwell (1983). Accordingly, 'the fluctuations of temperature and buoyancy are constantly being created on many scales at various rates. A patch of water responds to an increase in driving by increasing its stirring, perhaps by entraining neighbouring pieces of water'. The present flow configuration is akin to the latter mechanism and shows that the entrainment of neighbouring fluid is possible even if the stirring rate is constant. In the continuous creation hypothesis, the vertical scale for turbulence is considered to be L_T, whereas in the 'big-bang' view it is L_p. The vertical scale plays an important role in estimating certain quantities, for example, the vertical eddy diffusivity. With respect to each view, the eddy diffusivity becomes, $L_T^2 N$ or $L_p^2 N$. Since L_p is about 3.7 times larger than L_T, the two estimates differ by a factor of about fourteen. It is also noted that the determination of the sizes of oceanic patches is a difficult task. According to Caldwell (1983), L_p is usually determined by studying vertical temperature-gradient profiles for the extent of 'active' regions, i.e. regions in which the temperature gradient seems to remain non-zero while switching back and forth from positive to negative.

The present results show that such ratios as L_T/L_p, $(L_T)_{max}/L_p$ are strongly dependent on the evolutionary state of the patch and the mixing never goes to completion. By analysing the oceanic microstructure data of Desaubies & Gregg

(1981), Gregg (1987) has also concluded that oceanic mixing can never produce a completely mixed patch.

In the present work the growth of the patch is one dimensional as opposed to the three dimensionality of the geophysical situations. In the latter case the mixed fluid collapses to form a horizontal intrusion. The 'lost' fluid from the patch is replenished by return currents (if the stirring is sustained) and the process is more complicated. The present work can be considered as a first step towards an understanding of such intricate processes.

We wish to thank Mr. Leonard Montenegro for his able technical help, Professor D. F. Jankowski and G. Oth for their support in numerous ways and the referees for providing valuable input to the paper. The financial support of the Fluid Mechanics and Hydraulics Program of the National Science Foundation and the Office of Naval Research (Small-Scale Mixing and Arctic Sciences Programs) are gratefully acknowledged.

REFERENCES

BARANBLATT, G. I. 1982 Turbulence, heat and mass transfer in very stably stratified liquids. *Fluid Mech. Sov. Res.* **11**, (2), 75–94.

CALDWELL, D. R. 1983 Oceanic turbulence: big bangs or continuous creation? *J. Geophys. Res.* **88**, 7543–7550.

CARRUTHERS, D. J. & HUNT, J. C. R. 1986 Velocity fluctuations near an interface between a turbulent region and a stably stratified layer. *J. Fluid Mech.* **165**, 475–501.

CORRSIN, S. 1963 Turbulence: experimental methods. *Handbuch der Physik*, vol. 8, Stromungs Mechanik II, pp. 524–587. Springer.

CRAWFORD, W. R. 1986 A comparison of length-scales and decay times of turbulence in stably stratified flows. *J. Phys. Oceanogr.* **16**, 1847–1854.

DESAUBIES, Y. J. F. & GREGG, M. C. 1981 Reversible and irreversible finestructure. *J. Phys. Oceanogr.* **11**, 541–556.

DILLON, T. M. 1982 Vertical overturns: a comparison of Thorpe and Ozmidov length-scales. *J. Geophys. Res.* **87**, 9601–9613.

DILLON, T. M. 1984 The energies of overturning structures: implications for the theory of fossil turbulence. *J. Phys. Oceanogr.* **14**, 541–549.

DILLON, T. M. & PARK, M. M. 1987 The available potential energy of overturns as an indicator of mixing in the seasonal thermocline. *J. Geophys. Res.* **92**, C5, 5345–5353.

DUGAN, J. P. 1984 Towed observations of internal waves and patches of finescale turbulence. In *Internal Gravity Waves and Small Scale Turbulence*, Proc. Hawaiian winter workshop (ed. P. Muller & R. Pujalet), pp. 51–64.

DURAO, D. F. G., LAKER, J. & WHITELAW, J. H. 1980 Bias effects in laser Doppler anemometry. *J. Phys.* E: *Sci. Instrum.* **13**, 442–445.

E, X, & HOPFINGER, E. J. 1986 On mixing across an interface in stably stratified fluid. *J. Fluid Mech.* **166**, 227–244.

FERNANDO, H. J. S. 1988 The growth of a turbulent patch in a stratified fluid. *J. Fluid Mech.* **190**, 55–70.

FERNANDO, H. J. S. & LONG, R. R. 1983 The growth of a grid-generated turbulent mixed layer in a two-fluid system. *J. Fluid Mech.* **133**, 377–395.

FERNANDO, H. J. S. & LONG, R. R. 1985*a* The growth of a shear-free mixed layer in a linearly stratified fluid. *Phys. Fluids* **28** (10), 2999–3003.

FERNANDO, H. J. S. & LONG, R. R. 1985*b* On the nature of the entrainment interface of a two-layer fluid subjected to zero-mean-shear turbulence. *J. Fluid Mech.* **151**, 21–53.

FOLSE, R. F., COX, T. P. & SCHEXNAYDER, K. R. 1981 Measurements of the growth of a turbulently mixed layer in a linearly stratified fluid. *Phys. Fluids* **24** (3), 396–400.

GARGETT, A. E., OSBORN, T. R. & NASMYTH, P. W. 1984 Local isotropy and the decay of turbulence in a stratified fluid. *J. Fluid Mech.* **144**, 231–280.

GIBSON, C. H. 1980 Fossil turbulence, salinity and vorticity turbulence in the ocean. *Marine Turbulence Oceanographic Series*, vol. 16, pp. 221–257.

GIBSON, C. H. 1987 Oceanic turbulence: big bangs and continuous creation. *Physicochem. Hydrodyn.* **8** (1), 1–22.

GREGG, M. C. 1987 Diapycnal mixing in the thermocline: a review. *J. Geophys. Res.* **92**, 5249–5286.

HANNOUN, I. A., FERNANDO, H. J. S. & LIST, E. J. 1988 Turbulence structure near a sharp density interface. *J. Fluid Mech.* **189**, 189–209.

HEAD, M. J. 1983 The use of miniature four-electrode conductivity probes for high resolution measurement of turbulent density or temperature variations in salt-stratified water flows. PhD thesis, University of California, San Diego.

HOPFINGER, E. J. & LINDEN, P. F. 1982 Formation of thermocline in zero-mean-shear turbulence subjected to a stabilizing buoyancy flux. *J. Fluid Mech.* **114**, 157–173.

HOPFINGER, E. J. & TOLY, J.-A. 1976 Spatially decaying turbulence and its relation to mixing across density interfaces. *J. Fluid Mech.* **78**, 155–175.

HUNT, J. C. R., KAIMAL, J. C. & GAYNOR, J. E. 1985 Some observations of turbulence structure in stable layers. *Q. J. R. Met. Soc.* **111** (469), 793–816.

ITSWEIRE, E. C. 1984 Measurements of vertical overturns in a stably stratified turbulent flow. *Phys. Fluids* **27** (4), 764–766.

ITSWEIRE, E. C., HELLAND, K. N. & VAN ATTA, C. W. 1986 The evolution of grid generated turbulence in a stably stratified fluid. *J. Fluid Mech.* **162**, 299–338.

LIENHARD, J. H. & VAN ATTA, C. W. 1990 The decay of turbulence in thermally stratified flow. *J. Fluid Mech.* **210**, 57–112.

LONG, R. R. 1978*a* Theory of turbulence in a homogeneous fluid induced by an oscillating grid. *Phys. Fluids* **21** (10), 1887–1888.

LONG, R. R. 1978*b* A theory of mixing in a stably stratified fluid. *J. Fluid Mech.* **84**, 113–124.

MCDOUGALL, T. J. 1979 Measurements of turbulence in a zero-mean-shear mixed layer. *J. Fluid Mech.* **94**, 409–431.

MCLAUGHLIN, D. K. & TIELDERMAN, W. G. 1973 Biasing correction for individual realisation of laser anemometer measurements in turbulent flows. *Phys. Fluids* **16** (12), 2082–2088.

NASMYTH, P. W. 1970 Oceanic turbulence. PhD dissertation, University of British Columbia, Vancouver, Canada.

NASMYTH, P. W. 1972 Some observations on turbulence in the upper layers of the ocean. *Cons. Intl. Explor. Mer. Rapp. Proc. Verb.* **162**, 19–24.

OSTER, G. & YAMAMOTO, M. 1963 Density gradient techniques. *Chem. Rev.* **63**, 257–268.

OZMIDOV, R. V. 1965 On the turbulent exchange in a stably stratified ocean. *Bull. Acad. Sci. USSR Atmos. Ocean. Phys.* **1**, 493–497.

PEARSON, H. J., PUTTOCK, J. S. & HUNT, J. C. R. 1983 A statistical model of fluid-element motions and vertical diffusion in a homogeneous stratified turbulent flow. *J. Fluid Mech.* **129**, 219–249.

PHILLIPS, O. M. 1977 *The Dynamics of the Upper Ocean.* Cambridge University Press.

REDONDO, J. 1990 Mixing in stratified fluids. PhD thesis, University of Cambridge.

STILLINGER, D. C., HELLAND, K. N. & VAN ATTA, C. W. 1983 Experiments on the transition of homogeneous turbulence to internal waves in a stratified fluid. *J. Fluid Mech.* **131**, 91–122.

TENNEKES, H. & LUMLEY, J. L. 1973 *A First Course in Turbulence.* MIT. Press.

THOMPSON, S. M. & TURNER, J. S. 1975 Mixing across an interface due to turbulence generated by an oscillating grid. *J. Fluid Mech.* **67**, 349–368.

THORPE, S. A. 1977 Turbulence and mixing in a Scottish Loch. *Phil. Trans. Proc. R. Soc. Lond.* **A286**, 125–181.

TURNER, J. S. 1968 The influence of molecular diffusivity on turbulent entrainment across a density interface. *J. Fluid Mech.* **33**, 639–656.

YOON, K. & WARHAFT, Z. 1990 The evolution of grid-generated turbulence under conditions of stable thermal stratification. *J. Fluid Mech.* **215**, 601–638.